Homogenization of Metamaterial Surfaces and Slabs: The Crossed Wire Mesh Canonical Problem

Mário G. Silveirinha, *Member, IEEE,* and Carlos A. Fernandes, *Member, IEEE*

***Abstract*—The objective of this paper is to discuss the differences between the homogenization of a bulk metamaterial and the homogenization of a thin metamaterial slab (complex surface). To this end, we study the canonical problem of propagation of electromagnetic waves in a mesh of crossed metallic wires embedded in a dielectric slab. We prove that it may not be appropriate to characterize the complex surface with the same effective parameters as the bulk metamaterial and the usual boundary conditions. We develop a modified homogenization procedure that is suitable to homogenize the complex surface using the bulk material effective parameters. The results of our analytical model are compared with full wave numerical results, yielding an excellent agreement for long wavelengths. Our formulation is valid for slabs of arbitrary thickness. We hope that this work may contribute to a more profound understanding of the interaction of electromagnetic waves with the emerging metamaterials.**

***Index Terms*—Complex surfaces, homogenization theory, metamaterials, wire medium.**

I. Introduction

THE interaction of electromagnetic waves with structures periodic in two-dimensions (2-D) is an important problem in microwave engineering. These structures are known as frequency selective surfaces (FSS) [1] when used to control propagation properties. An example of an FSS is a periodic array consisting of conducting patches or aperture elements. Frequency selective surfaces find two major applications in microwave engineering, which explore their frequency filtering properties. The first one is the use of FSS as antenna radomes to better control electromagnetic wave transmission and scattering. The second one is in reflector antenna systems, where FSS reflectors are used to separate feeds of different frequency bands [1]. Recently it was also discovered that the high impedance surface formed by a capacitive FSS above a ground plane with interconnecting vias is the ideal ground plane for wireless applications with low profile antennas [2]-[3].

In general, the characterization of FSSs and other related complex surfaces requires intensive and time-consuming numerical simulations [1], which provide no understanding or insight into the physics of the problem. However, in the long wavelength limit, it is possible to characterize the interaction of electromagnetic waves with thin screens by using approximate boundary conditions. The idea is to impose an equivalent boundary condition on the thin screen. In general, the boundary condition relates the tangential electric field to the tangential magnetic field through a sheet impedance. When available, this approach provides an enormous reduction of the computational costs. It has been successfully applied to the characterization of the scattering from grids of wires standing in free-space [4], [5], grids of wires and strips near a dielectric interface [6]–[8], and arrays of scatterers with some rotational symmetry [9]. Also related with this topic is the asymptotic boundary condition (ASBC) proposed in [10], [11] to characterize grids of metal strips and corrugated surfaces. The ASBC boundary condition is asymptotic in the sense that it becomes more accurate the smaller the period of the grid is in terms of the wavelength. This approach is not limited to uniform periodicities of the strips and corrugations, and can be applied to finite structures as well.

The characterization of high impedance surfaces using homogenization methods has also been considered. In a recent paper [3], it was claimed that when the wavelength of operation is much larger than the period, the structure can be regarded as an artificial anisotropic magneto-dielectric material. This is a puzzling result since it raises the question: "To what extent can a thin 1-cell complex surface be regarded as a metamaterial?" Intuitively one would expect such interpretation to be possible only for *sufficiently* thick slabs. In fact, the characterization of a (unbounded) bulk metamaterial assumes interaction between a 3D-array of scatterers, while a complex surface is a thin 1-layer structure. For example, an FSS screen is typically 0.001λ thick [1]. A related question is: "Can the scattering by a complex surface be somehow characterized using the bulk metamaterial effective parameters?"

The objective of this paper is to contribute to clarify and answer the above questions through the study of a simple canonical problem: we will investigate the scattering of plane waves by a mesh of crossed metallic wires embedded in a dielectric. The thickness of the metamaterial slab can be arbitrary. We propose a new analytical homogenization procedure that allows the characterization of the scattering coefficients directly from the bulk material effective parameters. It will be shown that the analytical model describes very well the scattering of plane waves by the wire mesh for long wavelengths, even for wide incident angles and thin surfaces.

In addition, we homogenize the bulk metamaterial associated with the wire mesh (2-D-wire medium). Several methods have been proposed in the literature to compute the effective parameters of periodic composite materials (metallic or dielectric

Manuscript received November 29, 2003; revised September 12, 2004. This work was supported by the Fundação para Ciência e a Tecnologia under project POSI 34860/99.

M. G. Silveirinha is with the Electrical Engineering Department, Polo II da Universidade de Coimbra, 3030 Coimbra, Portugal (e-mail: mario.silveirinha@co.it.pt).

C. A. Fernandes is with the Instituto Superior Técnico, Technical University of Lisbon, 1049-001 Lisbon, Portugal (e-mail: carlos.fernandes@lx.it.pt).

Digital Object Identifier 10.1109/TAP.2004.840538

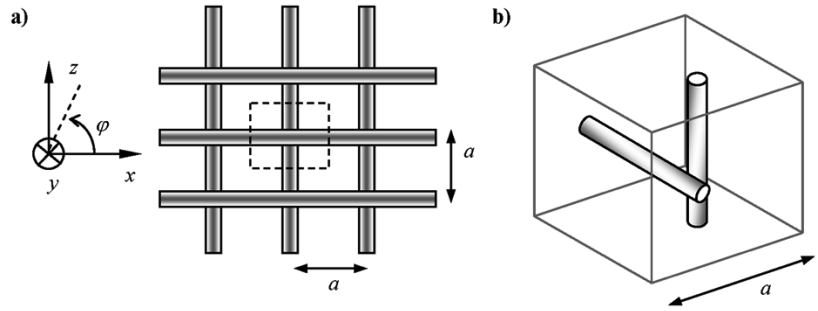

Fig. 1. (a) Geometry of the 2-D-wire medium; (b) Geometry of the unit cell.

crystals) [12]–[16]. For a detailed review of the homogenization methods see [16]. In this paper, we prove that the 2-D-wire medium can be modeled as an effective medium, provided that both spatial and frequency dispersion are taken into account. More specifically, the artificial medium is characterized by a permittivity dyadic that depends not only on the frequency, but also on the wave vector.

Apart from the studies presented in [15], [17], we are not aware of other works that model artificial media taking into account spatial dispersion. In [15], the reflection problem on an interface between a half space of vertical parallel wires (1-D-wire medium) and free space is solved for plane-wave excitation. In [17], it is found that the 1-D-wire medium can be described by a nonlocal dispersive uniaxial tensor. It is proven that the composite structure exhibits strong spatial dispersion even in the very large wavelength limit. None of these works investigates the scattering of plane waves by *thin slabs* of artificial material. The geometry of the artificial material considered in this paper is significantly different from that of [15] and [17]. Indeed, we investigate the interaction between electromagnetic waves and a mesh of crossed metallic wires (2-D-wire medium *slab*). We prove in this paper that the propagation characteristics in 1-D- and 2-D-wire media are rather different.

To a large extent our approach can be generalized to other geometries. We hope that the method may contribute to a more profound understanding of the interaction of electromagnetic waves with thin complex surfaces, and the relation between this problem and the homogenization of bulk materials. Unlike full wave numerical simulations, the computational effort required by our analytical formalism is negligible. The formalism only assumes that the permittivity of the bulk material is known, and that the propagation in the long wavelength limit can be described satisfactorily by the fundamental Floquet modes.

It is also important to point out the fundamental difference between our approach, and the classic approach which involves replacing the screen of scatterers by an equivalent boundary condition [4]–[9]. The difference is that our homogenization method relies on the effective parameters of the bulk material, for example the plasma frequency of the wire medium, which is a parameter defined uniquely for the unbounded structure. Conversely, the methods presented in [4]–[9] involve parameters that characterize uniquely the FSS screen. The method proposed in this paper can be applied in the homogenization of not only thin screens, but also metamaterial slabs of arbitrary thickness.

The outline of this paper is as follows. In Section II we characterize the propagation of electromagnetic waves in the (unbounded) 2-D-wire medium. We calculate the dispersion characteristic of the propagating modes and the average electromagnetic fields. Our theoretical model is validated using full wave numerical simulations. In Section III, we formulate and solve from an average perspective the problem of plane wave scattering by a mesh of crossed wires. We explain how to homogenize the problem taking into account the interface effects. We discuss the differences between the homogenization of the bulk artificial material, and the homogenization of an interface between two different media. In Section IV, we compare our analytical model with full wave numerical simulations obtained using the periodic method of moments (MoM). Finally, in Section V, some conclusions are drawn.

II. Permittivity Dyadic for the 2-D-Wire Medium

Before addressing in Section III the problem of scattering of plane waves by a mesh of crossed wires, we start by characterizing the propagating modes in the associated unbounded structure (a metallic crystal). The results will later be used to homogenize a *slab* of the artificial structure, as explained in the previous section.

The geometry of the periodic structure is depicted in Fig. 1. It consists of an array of metallic wires with infinite length embedded in a dielectric with permittivity ε_h. The wires are perfect electric conductors (PEC), and are oriented along the x and z directions. The z-oriented wires are centered at $(ma, na, 0)$, where m and n are generic integers and a is the distance between the wires (the lattice constant). The x-oriented wires are centered at $(0, na + a/2, ma)$, where m and n are defined as before. Thus, the spacing in the y direction between adjacent wires is half-lattice constant.

Equivalently, we can say that the metallic wires are arranged into a simple cubic lattice. The unit cell Ω contains sections of the wires as depicted in Fig. 1(b). The metallic crystal is obtained by periodic translations of the unit cell along three independent directions of space (the lattice primitive vectors). We denote the metallic region in the unit cell by D and its surface by ∂D. The outward unit vector normal to ∂D is $\hat{\boldsymbol{\nu}}$. The volume of the unit cell is $\mathrm{V_{cell}}$.

We denote the wire radius by r_w and admit that $r_w/a \ll 1$, i.e., that the wire radius is much smaller (at least ten times) than the lattice constant. Ahead, we will use this approximation to

model the artificial material as an effective medium. To begin with, we establish in next section some basic facts concerning the homogenization of the Maxwell equations.

A. Homogenization of the Maxwell-Equations

Let $(\mathbf{E},\mathbf{H})$ be an electromagnetic Floquet mode in a generic metallic crystal formed by a periodic array of metallic obstacles embedded in a dielectric with permittivity ε_h. The wave vector associated with $(\mathbf{E},\mathbf{H})$ is $\mathbf{k}=(k_x,k_y,k_z)$. In the dielectric region the electromagnetic field satisfies the (frequency dependent) Maxwell equations

$$\nabla\times\mathbf{E}=-j\beta\eta\mathbf{H} \tag{1a}$$

$$\nabla\times\eta\mathbf{H}=+j\beta\mathbf{E} \tag{1b}$$

where $\beta=\omega\sqrt{\mu_0\varepsilon_h}$ and $\eta=\sqrt{\mu_0/\varepsilon_h}$ are respectively the wave number and impedance of the host medium. Over the metallic interfaces the tangential component of the electric field vanishes, i.e., $\hat{\boldsymbol{\nu}}\times\mathbf{E}=0$. We define the average fields $\mathbf{E}_{\rm av}$ and $\mathbf{H}_{\rm av}$ as follows:

$$\mathbf{E}_{\rm av}=\frac{1}{\mathrm{V}_{\rm cell}}\int_\Omega \mathbf{E}(\mathbf{r})e^{+j\mathbf{k}\cdot\mathbf{r}}d^3\mathbf{r}$$

$$\mathbf{H}_{\rm av}=\frac{1}{\mathrm{V}_{\rm cell}}\int_\Omega \mathbf{H}(\mathbf{r})e^{+j\mathbf{k}\cdot\mathbf{r}}d^3\mathbf{r}. \tag{2}$$

Using (1) and the boundary conditions, it can be verified that

$$-\mathbf{k}\times\mathbf{E}_{\rm av}+\beta\eta\mathbf{H}_{\rm av}=0 \tag{3a}$$

$$\beta\mathbf{E}_{\rm av}+\mathbf{k}\times\eta\mathbf{H}_{\rm av}=\frac{j\eta}{\mathrm{V}_{\rm cell}}\int_{\partial D}\mathbf{J}_c e^{+j\mathbf{k}\cdot\mathbf{r}}\,ds \tag{3b}$$

where ∂D denotes the surface of the metallic region in the unit cell, and $\mathbf{J}_c=\hat{\boldsymbol{\nu}}\times\mathbf{H}$ is the electric current over the metallic surfaces. From (3), after some straightforward manipulations we obtain

$$[(\beta^2-k^2)\bar{\bar{\mathbf{I}}}+\mathbf{kk}]\cdot\mathbf{E}_{\rm av}=\frac{j\beta\eta}{\mathrm{V}_{\rm cell}}\int_{\partial D}\mathbf{J}_c e^{+j\mathbf{k}\cdot\mathbf{r}}\,ds \tag{4}$$

where $\bar{\bar{\mathbf{I}}}$ is the identity dyadic, and $k^2=\mathbf{k}\cdot\mathbf{k}$.

We seek to model the artificial medium using uniquely a permittivity dyadic. This is possible as long as the magnetic and higher dipole moments are negligible in the frequency band of interest. Within this hypothesis we can identify $\mathbf{H}_{\rm av}$ with the homogenized magnetic field (in general $\mathbf{H}_{\rm av}$ should be regarded as the average induction field normalized to μ_0). Thus, the (relative) permittivity dyadic $\overline{\overline{\varepsilon_r}}$ (normalized to the host permittivity) of the metallic crystal must be such that the following identity holds for every $\mathbf{k}$ and polarization

$$\varepsilon_h(\overline{\overline{\varepsilon_r}}-\bar{\bar{\mathbf{I}}})\cdot\mathbf{E}_{\rm av}=\frac{\varepsilon_h\eta}{j\beta\mathrm{V}_{\rm cell}}\int_{\partial D}\mathbf{J}_c e^{+j\mathbf{k}\cdot\mathbf{r}}\,ds. \tag{5}$$

Note that if we expand the term $\exp(j\mathbf{k}\cdot\mathbf{r})$ in the right-hand side of (5) in powers of the wave vector, the leading term is the polarization vector associated with the metallic obstacles (the average electric dipole moment in a unit cell). Substituting (5) in (4), we obtain the expected characteristic equation for the average field ([18, p. 202])

$$\beta^2\overline{\overline{\varepsilon_r}}\cdot\mathbf{E}_{\rm av}+(\mathbf{kk}-k^2\bar{\bar{\mathbf{I}}})\cdot\mathbf{E}_{\rm av}=0. \tag{6}$$

B. The Permittivity Dyadic

The objective of this section is to obtain the effective permittivity of the 2-D-wire medium. Under the assumption that $r_w/a\ll 1$, it was proved in [17] that the array of z-oriented wires can be described by the permittivity dyadic (normalized to the host permittivity)

$$\overline{\overline{\varepsilon_r}}=(\hat{\mathbf{u}}_x\hat{\mathbf{u}}_x+\hat{\mathbf{u}}_y\hat{\mathbf{u}}_y)+\varepsilon_{zz}\hat{\mathbf{u}}_z\hat{\mathbf{u}}_z,\quad \varepsilon_{zz}=1-\frac{\beta_0^2}{\beta^2-k_z^2}. \tag{7}$$

In the above, β_0 is the plasma wave number, and $\mathbf{k}=(k_x,k_y,k_z)$ is the wave vector. The result is expected to hold up to the second order in k_x and k_y (i.e., powers of k_x and k_y greater than two are neglected). Notice that the permittivity dyadic depends not only on the frequency, but also on the wave vector. Therefore, the effective medium exhibits both frequency and spatial dispersion. To a first order approximation, the plasma wave number satisfies [15]

$$(\beta_0 a)^2=\frac{2\pi}{\ln\left(\frac{a}{2\pi r_w}\right)+0.5275}. \tag{8}$$

This result can be trivially extended to the metallic crystal under study. In fact, provided that there is low interaction between the vertical and horizontal wires, it is reasonable to expect

$$\overline{\overline{\varepsilon_r}}=(\varepsilon_{xx}\hat{\mathbf{u}}_x\hat{\mathbf{u}}_x+\varepsilon_{zz}\hat{\mathbf{u}}_z\hat{\mathbf{u}}_z)+\hat{\mathbf{u}}_y\hat{\mathbf{u}}_y$$

$$\varepsilon_{i,i}=1-\frac{\beta_0^2}{\beta^2-k_i^2},\quad i=x,z. \tag{9}$$

Within this model, it is well-known ([18, p. 202] using a different notation) that we must have

$$\frac{k_x^2}{k^2-\beta^2\varepsilon_{xx}}+\frac{k_y^2}{k^2-\beta^2}+\frac{k_z^2}{k^2-\beta^2\varepsilon_{zz}}=1. \tag{10}$$

Assuming that the permittivity dyadic is given by (9), the above equation has five different solutions in β^2, which define the dispersion characteristic $\beta^2=\beta^2(\mathbf{k})$ of the electromagnetic modes. One of the solutions is $\beta^2=0$. It corresponds to static fields and so it does not contribute to the solution of the propagation problem. The other four solutions are the propagating modes. Unlike the number of solutions may suggest all the electromagnetic modes can be generated from only two families of Floquet waves. In fact, solving (10) for k_y, with ε_{xx} and ε_{zz} given by (9), we find that

$$k_y^2=k_{y,p\pm}^2=\beta^2-\left(\beta_0^2+k_x^2+k_z^2\pm\sqrt{L\left(k_x^2,k_z^2,\beta^2\right)}\right) \tag{11a}$$

$$\begin{aligned}L\left(k_x^2,k_z^2,\beta^2\right)=&\left(\beta^2-\beta_0^2-k_x^2-k_z^2\right)^2-\left[\beta^4\varepsilon_{xx}\varepsilon_{zz}\right.\\&-\beta^2k_x^2\varepsilon_{xx}(1+\varepsilon_{zz})-\beta^2k_z^2\varepsilon_{zz}(1+\varepsilon_{xx})\\&\left.+\varepsilon_{xx}k_x^4+\varepsilon_{zz}k_z^4+(\varepsilon_{xx}+\varepsilon_{zz})k_x^2k_z^2\right].\end{aligned} \tag{11b}$$

The above equation shows that there are only two solutions, $k_{y,p+}^2$ and $k_{y,p-}^2$, for k_y^2 (assuming that β, k_x, and k_z are fixed; the propagation constant k_y can be imaginary). Thus, for a fixed frequency the proposed model predicts that the plane wave solutions in the homogenized medium are either associated with the wave vector $\mathbf{k} = (k_x, k_{y,p+}, k_z)$ or with the wave vector $\mathbf{k} = (k_x, k_{y,p-}, k_z)$, where $k_{y,p\pm} = k_{y,p\pm}(\beta, k_x, k_z)$ is given by (11a). The indices p^+ and p^- identify the family of the modes.

As is well-known, the average electric field associated with an electromagnetic mode is given by ([18, p. 202] using a different notation and assuming that the field is not transverse)

$$\mathbf{E}_{\mathrm{av},p\pm} \propto \left(\frac{k_x}{k^2 - \beta^2 \varepsilon_{xx}}, \frac{k_y}{k^2 - \beta^2}, \frac{k_z}{k^2 - \beta^2 \varepsilon_{zz}} \right). \quad (12)$$

In the above, $\mathbf{E}_{\mathrm{av},p+}$ denotes the average field associated with the p^+ mode, and $\mathbf{E}_{\mathrm{av},p-}$ denotes the average field associated with the p^- mode. Since the wave vector must satisfy the dispersion characteristic (10), in (12) we have that $k_y = k_{y,p\pm}$, where $k_{y,p\pm}$ is defined by (11a). The average magnetic field is calculated using (3a).

So far the discussion was completely general. In what follows, in order to give some insight into the properties of the modes, we will characterize the solutions of (10) in the case $|\mathbf{k}|a \ll 1$.

As mentioned before, (10) has four solutions associated with propagating modes. Two of the solutions correspond to waves that start propagating in the static limit $\beta = 0$. One of the modes has the dispersion characteristic $\beta^2 \approx k_x^2 + k_z^2$, and polarization nearly parallel to the y direction. The other quasistatic mode interacts strongly with the metallic wires (the electric field is almost parallel to the plane of the wires), and for a sufficiently high frequency it is cutoff. Finally, there are two other solutions that correspond to modes that start propagating near the plasma frequency of the 1-D-wire medium. We claim that the dispersion characteristic of these two modes is given by

$$\beta^2 = \beta_{p\pm}^2 \approx \beta_{\mathrm{TM}}^2 \pm k_x k_z. \quad (13)$$

The proof of this result is given in the next paragraph. In the above $\beta_{\mathrm{TM}}^2 = \beta_0^2 + k^2$ is the dispersion characteristic of the transverse magnetic to z (TM) polarized mode in the 1-D-wire medium [15]. The proposed formulas hold up to the second order in $\mathbf{k}$ (i.e., powers of $\mathbf{k}$ greater than two are neglected), and in the vicinity of the plasma frequency.

Next, we justify why (13) is compatible with (9). In fact, expanding the auxiliary function L, defined by (11b), in a power series around the point $(k_x^2, k_z^2, \beta^2) = (0, 0, \beta_0^2)$, and neglecting powers of k_x^2, k_z^2 and $\beta^2 - \beta_0^2$ greater than two, we obtain that

$$L\left(k_x^2, k_z^2, \beta^2\right) \approx k_x^2 k_z^2. \quad (14)$$

Substituting the above equation into (11a), we conclude that to a first order approximation $\beta_{p\pm}^2$ indeed verifies (10) in the vicinity of the plasma frequency. In Fig. 2, we depict the theoretical wave normal contours $\beta_{p\pm}^2 = \mathrm{const}$. Note that $\beta_{p+}^2(k_x, k_y, k_z) = \beta_{p-}^2(-k_z, k_y, k_x)$ as a consequence of the medium being invariant under a rotation of 90° around the y axis.

Next, we find approximate formulas for the polarization of the fields. Using (9) and (13), and neglecting powers of $\mathbf{k}$ greater than two, we find that

$$k^2 - \beta_{p\pm}^2 \varepsilon_{i,i} \approx k_i^2 - (\pm k_x k_z), \quad i = x, z \quad (15a)$$

$$k_y / \left(k^2 - \beta_{p\pm}^2\right) \approx -k_y / \beta_0^2. \quad (15b)$$

Substituting the above equations in (12), we obtain that to a first approximation

$$\mathbf{E}_{\mathrm{av},p\pm} \approx E_0 \left(-1, \frac{k_y (k_x \mp k_z)}{\beta_0^2}, \pm 1 \right) \quad (16)$$

where E_0 is an arbitrary normalization constant.

From (16), we see that the average electric field is almost contained in the xoz plane. To a first order approximation, the polarization of the p^+ mode is along the direction $\varphi = -45°$ (see Fig. 1), and the polarization of the p^- mode is along the direction $\varphi = +45°$. It is important to stress that (13) and (16) are only valid for modes that propagate near the plasma frequency and as long as $|\mathbf{k}|a \ll 1$.

The previous results clearly show that the electrodynamics of the 2-D-wire medium is very different from that of the 1-D-wire medium (the array of vertical wires). Indeed both the wave normal contours and the polarization of the fields are completely different in the two periodic structures.

C. Numerical Validation

In order to validate the proposed model, the dispersion characteristic of the 2-D-wire medium was numerically obtained using the full wave method proposed by the authors of this paper in [19]. The numerical results refer to wires with radius $r_w = 0.01a$.

We computed the resonant frequencies of the plasma modes for $\mathbf{k} = 0.1(\cos\varphi, 0, \sin\varphi)\pi/a$ (the φ angle is the direction of the wave vector relative to the x axis). From (13), we expect that $(\beta_{p+}a)^2 - (\beta_{p-}a)^2 \approx 2(k_x a)(k_z a)$. This term is the most important difference in the dispersion characteristic, comparing with the 1-D-wire medium. In Fig. 3 the full wave numerical results (full line) are compared with the theoretical predictions from the proposed model (dashed line), showing good agreement. The dispersion characteristic of each individual mode is also in good agreement with (13) (in order to simplify the figure, only the difference between the two propagation constants was plotted).

In addition, using also the numerical method proposed in [19], we averaged the electromagnetic modes to obtain the polarization of the homogenized fields. We computed the angle that the average electric field makes with the x axis as a function of φ (the direction of the wave vector), and compared it with (16). The result for the p^+ mode is depicted in Fig. 4 and shows good agreement, especially for directions not too close to the x- and z axes. The discrepancy along the wire axes is not very important since the polarization of the plasma modes is degenerate along these directions. Similar results are obtained for the p^- mode.

The previous results demonstrate that our theoretical model accurately describes the propagation of electromagnetic waves in the 2-D-wire medium from an average perspective.

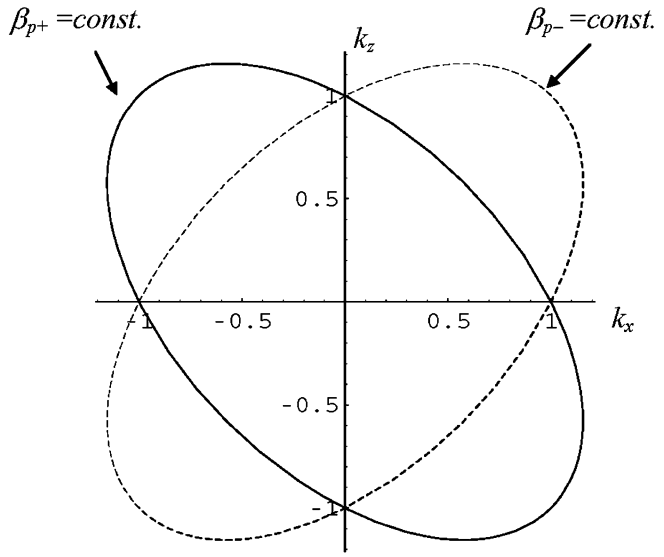

Fig. 2. Normalized wave normal contours for $k_y = 0$. Full line: $\beta_{p+} = \text{const}$. Dashed line: $\beta_{p-} = \text{const}$.

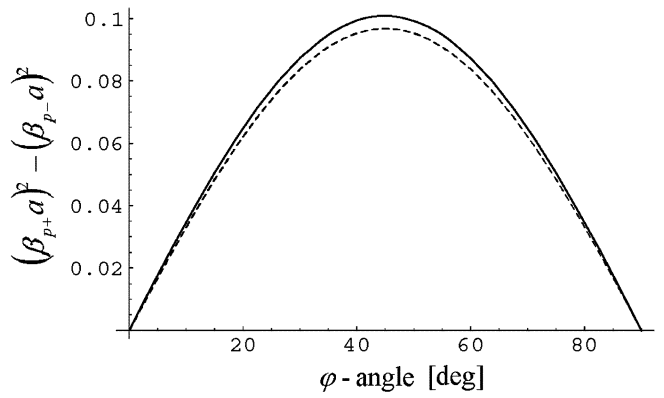

Fig. 3. Plot of $\beta_{p+}^2 - \beta_{p-}^2$ as a function of the φ-angle. Full line: numerical results. Dashed line: theoretical results. The wire radius is $r_w = 0.01a$.

III. Homogenization of a 2-D-Wire Medium Slab

In this section, we investigate the incidence of plane waves in a *slab* of the 2-D-wire medium. The geometry is depicted in Fig. 5. The slab consists of a finite number of layers, N_L, of crossed wires. The thickness of each layer is a (the lattice constant). As in the previous section, the wires are embedded in dielectric material with permittivity ε_h. The metamaterial slab stands in free-space.

Each layer contains two sets of wires: one set of vertical wires and one set of horizontal wires. The vertical wires in the leftmost layer are located at $y = y_z$, whereas the horizontal wires in the leftmost layer are located at $y = y_x$, where $y_x = y_z + 0.5a$. The interfaces of the metamaterial slab are coincident with the interfaces of the dielectric host (dashed lines in Fig. 5). The leftmost interface is at y'_L and the rightmost interface is at $y'_R = y'_L + N_L a$. The interfaces are, of course, normal to the y direction. Obviously, the definition of y'_L is rather arbitrary if $\varepsilon_h = \varepsilon_0$, i.e., if the wires stand in free-space.

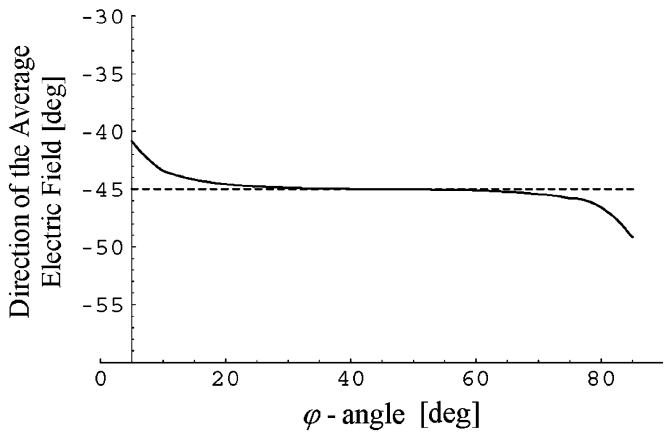

Fig. 4. Direction of the average electric field as a function of the φ-angle. Full line: numerical results. Dashed line: theoretical results. The wire radius is $r_w = 0.01a$.

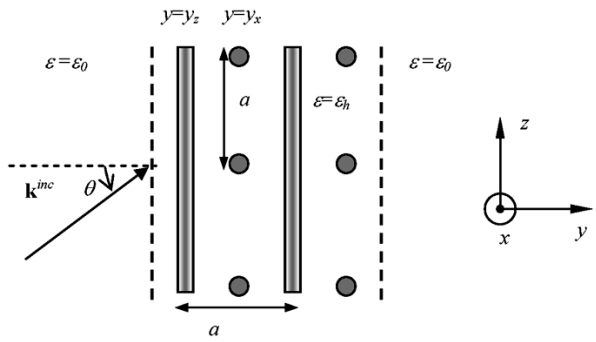

Fig. 5. Slab of the 2-D-wire medium with two layers. The dashed lines represent the interfaces.

A possible choice is $y'_L = y_z - 0.25a$. The formalism developed in this section works equally well for other choices (e.g., $y'_L = y_z - \delta_y, 0 < \delta_y < 0.5a$).

As depicted in Fig. 5, a free-space plane wave with wave vector $\mathbf{k}^{\text{inc}} = \mathbf{k}^{\text{inc}}_{//} + k_y^{\text{inc}}\hat{\mathbf{u}}_y$ impinges on the left interface, where $\mathbf{k}^{\text{inc}}_{//} = (k_x^{\text{inc}}, 0, k_z^{\text{inc}})$. The objective is to obtain an analytical model that allows the calculation of the scattered far field. The incident field is assumed to be either a TE or TM plane wave relative to the plane of incidence (defined by $\mathbf{k}^{\text{inc}}$ and by the normal to the interface $\hat{\mathbf{u}}_y$), more specifically $\mathbf{E}^{\text{inc}} = \mathbf{E}^{\text{TE}}(\mathbf{k}^{\text{inc}}; y'_L)$ or $\mathbf{E}^{\text{inc}} = \mathbf{E}^{\text{TM}}(\mathbf{k}^{\text{inc}}; y'_L)$ where the generic TE and TM waves are of the form

$$\mathbf{E}^{\text{TE}}(\mathbf{k}; y') = \mathbf{E}^{\text{TE}}_{\text{av}}(\mathbf{k}) e^{-j\mathbf{k}\cdot(\mathbf{r}-\mathbf{r}')}, \quad \text{where}$$
$$\mathbf{E}^{\text{TE}}_{\text{av}}(\mathbf{k}) = \frac{\hat{\mathbf{u}}_y \times \mathbf{k}}{|\hat{\mathbf{u}}_y \times \mathbf{k}|} \quad [\text{V/m}] \tag{17a}$$
$$\mathbf{E}^{\text{TM}}(\mathbf{k}; y') = \mathbf{E}^{\text{TM}}_{\text{av}}(\mathbf{k}) e^{-j\mathbf{k}\cdot(\mathbf{r}-\mathbf{r}')}, \quad \text{where}$$
$$\mathbf{E}^{\text{TM}}_{\text{av}}(\mathbf{k}) = -\frac{\mathbf{k}}{\hat{\beta}} \times \left(\frac{\hat{\mathbf{u}}_y \times \mathbf{k}}{|\hat{\mathbf{u}}_y \times \mathbf{k}|} \right) \quad [\text{V/m}] \tag{17b}$$

and $\hat{\beta} = \omega\sqrt{\mu_0 \varepsilon_0}$ is the free-space wave number, $\mathbf{k} \cdot \mathbf{k} = \hat{\beta}^2$ and $\mathbf{r}' = (0, y', 0)$.

A. Modal Formulation of the Problem

Next, we formulate the scattering problem using a modal approach. As is well-known [1], the total electric field $\mathbf{E}$ for $y < y'_L$ can be written as

$$\mathbf{E} = \mathbf{E}^{\text{inc}} + \sum_{\bar{\mathbf{J}}} \rho_{\bar{\mathbf{J}}}^{\text{TE}} \mathbf{E}^{\text{TE}}\left(\mathbf{k}_{\bar{\mathbf{J}}}^{\text{ref}}; y'_L\right) + \rho_{\bar{\mathbf{J}}}^{\text{TM}} \mathbf{E}^{\text{TM}}\left(\mathbf{k}_{\bar{\mathbf{J}}}^{\text{ref}}; y'_L\right)$$
$$\mathbf{k}_{\bar{\mathbf{J}}}^{\text{ref}} = \mathbf{k}_{\bar{\mathbf{J}},//} - k_{\bar{\mathbf{J}},y}\hat{\mathbf{u}}_y \tag{18}$$

where we have

$$\mathbf{k}_{\bar{\mathbf{J}},//} = \mathbf{k}_{//}^{\text{inc}} + \left(\frac{2\pi}{a} j_1, 0, \frac{2\pi}{a} j_2\right)$$
$$k_{\bar{\mathbf{J}},y} = -j\sqrt{|\mathbf{k}_{\bar{\mathbf{J}},//}|^2 - \hat{\beta}^2} \tag{19}$$

and $\bar{\mathbf{J}} = (j_1, j_2)$ is an arbitrary multi-index of integers, and $\rho_{\bar{\mathbf{J}}}^{\text{TE}}$ and $\rho_{\bar{\mathbf{J}}}^{\text{TM}}$ are the (unknown) reflection coefficients.

Similarly, the total electric field for $y > y'_R$, can be written as

$$\mathbf{E} = \sum_{\bar{\mathbf{J}}} t_{\bar{\mathbf{J}}}^{\text{TE}} \mathbf{E}^{\text{TE}}\left(\mathbf{k}_{\bar{\mathbf{J}}}^{tx}; y'_R\right) + t_{\bar{\mathbf{J}}}^{\text{TM}} \mathbf{E}^{\text{TM}}\left(\mathbf{k}_{\bar{\mathbf{J}}}^{tx}; y'_R\right)$$
$$\mathbf{k}_{\bar{\mathbf{J}}}^{tx} = \mathbf{k}_{\bar{\mathbf{J}},//} + k_{\bar{\mathbf{J}},y}\hat{\mathbf{u}}_y \tag{20}$$

where $t_{\bar{\mathbf{J}}}^{\text{TE}}$ and $t_{\bar{\mathbf{J}}}^{\text{TM}}$ are the (unknown) transmission coefficients.

In the 2-D wire medium slab, $y'_L < y < y'_R$, we can expand the electromagnetic fields in Floquet modes of the unbounded artificial material. In general, the Floquet modes have complex wave vector, and are associated with the host-medium wave number β. The modes that propagate in the positive y direction are denoted by $\mathbf{E}_n^f$, and are associated with the wave vector $\mathbf{k}_n^f$, where n is the index that identifies the mode. Similarly, the modes that propagate in the negative y direction are denoted by $\mathbf{E}_n^b$ and are associated with the wave vector $\mathbf{k}_n^b$. The projection of $\mathbf{k}_n^f$ and $\mathbf{k}_n^b$ into the interface (i.e., the *xoz* plane) is $\mathbf{k}_{//}^{\text{inc}}$, i.e., the transversal component of the incident wave vector is preserved. We follow the rule that wave vectors that differ by translations along the reciprocal lattice primitive vectors are equivalent [20]. In general, the electromagnetic modes $\mathbf{E}_n^f$ and $\mathbf{E}_n^b$ belong to the "complex" band structure of the artificial material. An electromagnetic mode belongs to the "real" band structure, only if its wave vector is real. We also note that $\mathbf{E}_n^f$ and $\mathbf{E}_n^b$ are basically the analog of the free-space electromagnetic modes used in the expansions (18) and (20). From the previous discussion, we conclude that in the wire medium slab we can write

$$\mathbf{E} = \sum_n c_n^f \mathbf{E}_n^f + \sum_n c_n^b \mathbf{E}_n^b \tag{21}$$

where c_n^f and c_n^b are the (unknown) coefficients of the expansion (the amplitudes of the forward and backward waves).

As is well-known, the unknown coefficients can be obtained by matching the tangential components of the electric and magnetic fields at the interfaces $y = y'_L$ and $y = y'_R$. Thus, we obtain four independent vector equations, two for each interface. For example, the continuity of the tangential electric field at $y = y'_L$ gives

$$\hat{\mathbf{u}}_y \times \left[\mathbf{E}^{\text{inc}} + \sum_{\bar{\mathbf{J}}} \rho_{\bar{\mathbf{J}}}^{\text{TE}} \mathbf{E}^{\text{TE}}\left(\mathbf{k}_{\bar{\mathbf{J}}}^{\text{ref}}; y'_L\right) + \rho_{\bar{\mathbf{J}}}^{\text{TM}} \mathbf{E}^{\text{TM}}\left(\mathbf{k}_{\bar{\mathbf{J}}}^{\text{ref}}; y'_L\right)\right]$$
$$= \hat{\mathbf{u}}_y \times \left[\sum_n c_n^f \mathbf{E}_n^f + \sum_n c_n^b \mathbf{E}_n^b\right]. \tag{22}$$

The above equation must hold for an arbitrary x and z in the plane $y = y'_L$.

B. Homogenization of the Problem

In this section, we explain how the scattering problem previously discussed can be homogenized. Our objective is to simplify the equations that establish the boundary conditions, e.g., (22). Indeed, these equations involve an infinite number of unknowns: the reflection and transmission coefficients. The idea is to obtain a simplified system with only a few unknowns. To this end, we multiply both sides of (22) by $\exp(j\mathbf{k}_{//}^{\text{inc}} \cdot \mathbf{r})$, and then integrate the resulting equation over the transversal unit cell (i.e., in the x- and z-coordinates). More specifically, each vector field is averaged as follows:

$$\mathbf{F}_{\text{av,T}}(y) = \frac{1}{\text{A}_{\text{cell}}} \int_{-a/2}^{a/2} \int_{-a/2}^{a/2} \mathbf{F}(x, y, z) e^{j\mathbf{k}_{//}^{\text{inc}} \cdot \mathbf{r}} dx dz. \tag{23}$$

In the above equation, $\mathbf{F}$ stands for a generic vector field, and $\text{A}_{\text{cell}} = a^2$ is the area of the transversal unit cell.

Since $\mathbf{E}_{\text{av,T}}^{\text{TM}}(\mathbf{k}_{\bar{\mathbf{J}}}^{\text{ref}})$ and $\mathbf{E}_{\text{av,T}}^{\text{TE}}(\mathbf{k}_{\bar{\mathbf{J}}}^{\text{ref}})$ vanish for $\bar{\mathbf{J}} \neq (0,0)$, we obtain from (22) that

$$\hat{\mathbf{u}}_y \times \left[\mathbf{E}_{\text{av}}^{\text{inc}} + \rho_{\mathbf{0}}^{\text{TE}} \mathbf{E}_{\text{av}}^{\text{TE}}(\mathbf{k}^{\text{ref}}) + \rho_{\mathbf{0}}^{\text{TM}} \mathbf{E}_{\text{av}}^{\text{TM}}(\mathbf{k}^{\text{ref}})\right]$$
$$= \hat{\mathbf{u}}_y \times \left[\sum_n c_n^f \mathbf{E}_{n,\text{av,T}}^f(y'_L) + \sum_n c_n^b \mathbf{E}_{n,\text{av,T}}^b(y'_L)\right] \tag{24}$$

where $\mathbf{k}^{\text{ref}}$ stands for $\mathbf{k}_{\bar{\mathbf{J}}}^{\text{ref}}$ calculated for $\bar{\mathbf{J}} = (0,0)$, and $\mathbf{E}_{\text{av}}^{\text{TE}}$ and $\mathbf{E}_{\text{av}}^{\text{TM}}$ are given by (17). So, the proposed procedure reduces the infinite sum in the left-hand side of (22) to three unique terms. However, the right-hand side of (24) has still an infinite number of terms. To circumvent this problem, we assume that the unique electromagnetic modes in the 2-D-wire medium that have significant spectral content at the wave vector $\mathbf{k}_{//}^{\text{inc}}$ belong to the two families of Floquet modes (p^+ and p^- modes) characterized in Section II. This assumption seems reasonable, because in the long wavelength limit only these modes can propagate in the unbounded structure. Since the transversal component of the incident wave vector is preserved, for a given frequency there are four independent modes with the required properties. Two modes, $\mathbf{E}_{p+}(\mathbf{r}; \mathbf{k}_{p+}^f)$ and $\mathbf{E}_{p-}(\mathbf{r}; \mathbf{k}_{p-}^f)$ propagate in the positive y direction (forward), and are associated with the wave vectors

$$\mathbf{k}_{p\pm}^f = \mathbf{k}_{//}^{\text{inc}} + k_{y,p\pm}\hat{\mathbf{u}}_y \tag{25}$$

where $k_{y,p\pm} = -j\sqrt{-k_{y,p\pm}^2}$ is calculated using (11a) with $k_x = k_x^{\text{inc}}$ and $k_z = k_z^{\text{inc}}$. The other two modes, $\mathbf{E}_{p+}(\mathbf{r}; \mathbf{k}_{p+}^b)$

and $\mathbf{E}_{p-}(\mathbf{r};\mathbf{k}^b_{p-})$, propagate in the negative y direction (backward), and are associated with the wave vectors

$$\mathbf{k}^b_{p\pm} = \mathbf{k}^{\rm inc}_{//} - k_{y,p\pm}\hat{\mathbf{u}}_y. \tag{26}$$

Using the hypothesis enunciated above, we conclude that (24) simplifies to

$$\begin{aligned}\hat{\mathbf{u}}_y \times &\left[\mathbf{E}^{\rm inc}_{\rm av} + \rho^{\rm TE}_{\mathbf{0}}\mathbf{E}^{\rm TE}_{\rm av}(\mathbf{k}^{\rm ref}) + \rho^{\rm TM}_{\mathbf{0}}\mathbf{E}^{\rm TM}_{\rm av}(\mathbf{k}^{\rm ref})\right] \\ &= \hat{\mathbf{u}}_y \times \Big[c^f_{p+}\mathbf{E}_{{\rm av},{\rm T},p+}\left(y'_L;\mathbf{k}^f_{p+}\right) \\ &\quad + c^f_{p-}\mathbf{E}_{{\rm av},{\rm T},p-}\left(y'_L;\mathbf{k}^f_{p,-}\right) \\ &\quad + c^b_{p+}\mathbf{E}_{{\rm av},{\rm T},p+}\left(y'_L;\mathbf{k}^b_{p+}\right) + c^b_{p-}\mathbf{E}_{{\rm av},{\rm T},p-}\left(y'_L;\mathbf{k}^b_{p-}\right)\Big].\end{aligned} \tag{27a}$$

The three remaining equations that guarantee the continuity of tangential components of the electric and magnetic fields at the interfaces are homogenized in a similar manner, resulting in

$$\begin{aligned}\hat{\mathbf{u}}_y \times &\left[\mathbf{H}^{\rm inc}_{\rm av} + \rho^{\rm TE}_{\mathbf{0}}\mathbf{H}^{\rm TE}_{\rm av}(\mathbf{k}^{\rm ref}) + \rho^{\rm TM}_{\mathbf{0}}\mathbf{H}^{\rm TM}_{\rm av}(\mathbf{k}^{\rm ref})\right] \\ &= \hat{\mathbf{u}}_y \times \Big[c^f_{p+}\mathbf{H}_{{\rm av},{\rm T},p+}\left(y'_L;\mathbf{k}^f_{p+}\right) \\ &\quad + c^f_{p-}\mathbf{H}_{{\rm av},{\rm T},p-}\left(y'_L;\mathbf{k}^f_{p-}\right) \\ &\quad + c^b_{p+}\mathbf{H}_{{\rm av},{\rm T},p+}\left(y'_L;\mathbf{k}^b_{p+}\right) + c^b_{p-}\mathbf{H}_{{\rm av},{\rm T},p-}\left(y'_L;\mathbf{k}^b_{p-}\right)\Big]\end{aligned} \tag{27b}$$

$$\begin{aligned}\hat{\mathbf{u}}_y \times &\left[t^{\rm TE}_{\mathbf{0}}\mathbf{E}^{\rm TE}_{\rm av}(\mathbf{k}^{\rm inc}) + t^{\rm TM}_{\mathbf{0}}\mathbf{E}^{\rm TM}_{\rm av}(\mathbf{k}^{\rm inc})\right] \\ &= \hat{\mathbf{u}}_y \times \Big[c^f_{p+}\mathbf{E}_{{\rm av},{\rm T},p+}\left(y'_R;\mathbf{k}^f_{p+}\right) \\ &\quad + c^f_{p-}\mathbf{E}_{{\rm av},{\rm T},p-}\left(y'_R;\mathbf{k}^f_{p-}\right) \\ &\quad + c^b_{p+}\mathbf{E}_{{\rm av},{\rm T},p+}\left(y'_R;\mathbf{k}^b_{p+}\right) + c^b_{p-}\mathbf{E}_{{\rm av},{\rm T},p-}\left(y'_R;\mathbf{k}^b_{p-}\right)\Big]\end{aligned} \tag{27c}$$

$$\begin{aligned}\hat{\mathbf{u}}_y \times &\left[t^{\rm TE}_{\mathbf{0}}\mathbf{H}^{\rm TE}_{\rm av}(\mathbf{k}^{\rm inc}) + t^{\rm TM}_{\mathbf{0}}\mathbf{H}^{\rm TM}_{\rm av}(\mathbf{k}^{\rm inc})\right] \\ &= \hat{\mathbf{u}}_y \times \Big[c^f_{p+}\mathbf{H}_{{\rm av},{\rm T},p+}\left(y'_R;\mathbf{k}^f_{p+}\right) \\ &\quad + c^f_{p-}\mathbf{H}_{{\rm av},{\rm T},p-}\left(y'_R;\mathbf{k}^f_{p-}\right) \\ &\quad + c^b_{p+}\mathbf{H}_{{\rm av},{\rm T},p+}\left(y'_R;\mathbf{k}^b_{p+}\right) + c^b_{p-}\mathbf{H}_{{\rm av},{\rm T},p-}\left(y'_R;\mathbf{k}^b_{p-}\right)\Big]\end{aligned} \tag{27d}$$

where $\mathbf{H}^{\rm TE}_{\rm av}$ and $\mathbf{H}^{\rm TM}_{\rm av}$ are obtained from $\mathbf{E}^{\rm TE}_{\rm av}$ and $\mathbf{E}^{\rm TM}_{\rm av}$ using (3a) with the free-space wave number and the free-space impedance.

Each of the vector equations in (27) generates two independent scalar equations. So, we obtain an 8×8 linear system with eight unknowns (the reflection and transmission coefficients, and the amplitudes of the waves inside the homogenized slab). The linear system can be solved numerically (or even analytically, although the expressions result rather cumbersome) provided we known the homogenized fields $\mathbf{E}_{{\rm av},{\rm T},p\pm}(y;\mathbf{k})$, and $\mathbf{H}_{{\rm av},{\rm T},p\pm}(y;\mathbf{k})$. These fields are obtained by inserting $(\mathbf{E}_{p\pm},\mathbf{H}_{p\pm})$ into (23), and are derived in the next section.

It is important to remember that the averaging in (23) only affects the transversal coordinates, i.e., x and z. Therefore, $(\mathbf{E}_{{\rm av},{\rm T},p\pm},\mathbf{H}_{{\rm av},{\rm T},p\pm})$ differ from the average fields $(\mathbf{E}_{{\rm av},p\pm},\mathbf{H}_{{\rm av},p\pm})$ obtained in Section II. In fact, from definition (2), $(\mathbf{E}_{{\rm av},p\pm},\mathbf{H}_{{\rm av},p\pm})$ are obtained by averaging the electromagnetic modes $(\mathbf{E}_{p\pm},\mathbf{H}_{p\pm})$ over the whole unit cell, i.e., in this case the averaging affects not only the transversal coordinates, but also the longitudinal coordinate y.

In general, it would be a mistake to identify $(\mathbf{E}_{{\rm av},{\rm T},p\pm},\mathbf{H}_{{\rm av},{\rm T},p\pm})$ with $(\mathbf{E}_{{\rm av},p\pm},\mathbf{H}_{{\rm av},p\pm})$. In fact, these fields may be substantially different, especially if the lattice constant is not significantly smaller than the wavelength. For example, if such approximation were made in the case under study, we would obtain a complete disagreement between the cross-polarization level predicted by the theoretical model and the full wave numerical results. We will discuss this aspect with more detail in Section IV. In what follows, we derive the correct relation between the different fields.

C. The Average Fields

The objective of this section is to calculate the (transversal) average fields defined in the previous section. The formulation presented here, is rather general and can be easily extended to other periodic structures with metallic planar (or almost planar) inclusions (at least when the unit cell has a single metallic inclusion). This geometry is rather common in FSS screens.

Let $(\mathbf{E},\mathbf{H})$ denote a generic electromagnetic mode in the 2-D-wire medium [for example the mode $(\mathbf{E}_{p+},\mathbf{H}_{p+})$], and let $(\mathbf{E}_{{\rm av},{\rm T}},\mathbf{H}_{{\rm av},{\rm T}})$ stand for the field obtained by inserting $(\mathbf{E},\mathbf{H})$ into (23). In what follows, we relate $\mathbf{E}_{{\rm av},{\rm T}}(y;\mathbf{k})$ with $\mathbf{E}_{\rm av}$ defined by (2).

To begin with, we note that $\mathbf{E}_{{\rm av},{\rm T}}(y;\mathbf{k})$ is pseudo-periodic in y, and thus can be expanded into a Fourier series

$$\mathbf{E}_{{\rm av},{\rm T}}(y;\mathbf{k}) = \sum_n \mathbf{E}_{{\rm av},n}e^{-j(k_y+\frac{2\pi}{a)n}y} \tag{28a}$$

$$\begin{aligned}\mathbf{E}_{{\rm av},n} &= \frac{1}{a}\int_{-a/2}^{a/2}\mathbf{E}_{{\rm av},{\rm T}}(y;\mathbf{k})e^{-j(k_y+\frac{2\pi}{a)n}y}dy \\ &= \frac{1}{{\rm V}_{\rm cell}}\int_{\Omega}\mathbf{E}(\mathbf{r})e^{+j\mathbf{k}_n\cdot\mathbf{r}}d^3\mathbf{r}.\end{aligned} \tag{28b}$$

In the above $\mathbf{k}_n = \mathbf{k}+(0,n2\pi/a,0)$, and n is a generic integer. We note that $\mathbf{E}_{{\rm av},0} = \mathbf{E}_{\rm av}$.

Since $\mathbf{k}_n$ differs from $\mathbf{k}$ by a reciprocal lattice vector, formulas (3)–(4) derived in Section II remain valid if we replace $\mathbf{k}$ by $\mathbf{k}_n$ and $\mathbf{E}_{\rm av}$ by $\mathbf{E}_{{\rm av},n}$. Thus, by inverting the dyadic in the left-hand side of (4), we obtain

$$\mathbf{E}_{{\rm av},n} = -j\beta\eta\bar{\bar{\mathbf{G}}}(\mathbf{k}_n)\cdot\int_{\partial D}\mathbf{J}_c(\mathbf{r}')e^{+j\mathbf{k}_n\cdot\mathbf{r}'}ds' \tag{29a}$$

$$\bar{\bar{\mathbf{G}}}(\mathbf{k}) = \frac{1}{\beta^2}\frac{1}{{\rm V}_{\rm cell}}\frac{\beta^2\bar{\bar{\mathbf{I}}}-\mathbf{k}\mathbf{k}}{k^2-\beta^2}. \tag{29b}$$

At this point, we note that the wire inclusions are quasiplanar, i.e., quasicontained in planes parallel to the xoz plane. This property follows from the assumption that the wire radius is small. In analogy with the geometry of Fig. 5, the vertical wires in the 2-D-wire medium are quasicontained in the planes $y = y_z + na$. Similarly, the horizontal wires are quasicontained in

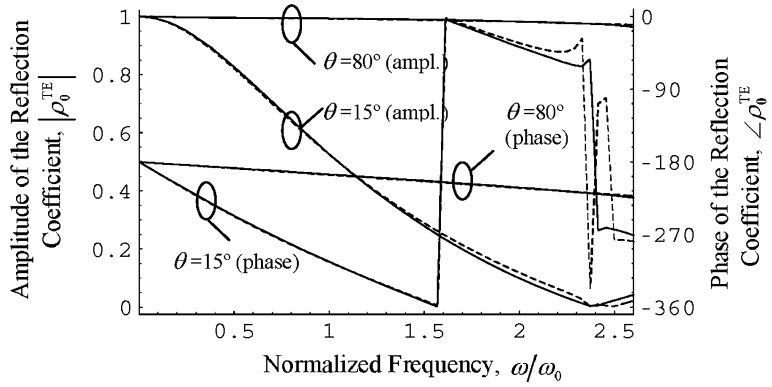

Fig. 6. Reflection coefficient (co-polarized wave) versus normalized frequency: TE-incidence and $\varphi = 45°, \theta = 15°, 80°; \varepsilon_h = \varepsilon_0$. Full line: numerical results. Dashed line: analytical model.

the planes $y = y_x + na$. Within this approximation, the integral in (29a) simplifies to

$$\int_{\partial D} \mathbf{J}_c(\mathbf{r}')e^{+j\mathbf{k}_n\cdot\mathbf{r}'}\,ds' \approx \sum_{i=x,z} e^{j\frac{2\pi}{a}ny_i} \int_{\partial D_i} \mathbf{J}_c(\mathbf{r}')e^{+j\mathbf{k}\cdot\mathbf{r}'}\,ds' \tag{30}$$

where ∂D_x and ∂D_z are, respectively, the surface of the wire element inside the unit cell that is oriented in the x- and z direction. Assuming also that the current flows along the wire axes, it is clear that the previous equation can be written as

$$\int_{\partial D} \mathbf{J}_c(\mathbf{r}')e^{+j\mathbf{k}_n\cdot\mathbf{r}'}\,ds' \approx \left(e^{j\frac{2\pi}{a}ny_x}\hat{\mathbf{u}}_x\hat{\mathbf{u}}_x + e^{j\frac{2\pi}{a}ny_z}\hat{\mathbf{u}}_z\hat{\mathbf{u}}_z\right) \cdot \int_{\partial D} \mathbf{J}_c(\mathbf{r}')e^{+j\mathbf{k}\cdot\mathbf{r}'}\,ds'. \tag{31}$$

Substituting (31) in (29a) and using (5), we obtain the important result

$$\mathbf{E}_{\mathrm{av},n} = \beta^2 \mathrm{V}_{\mathrm{cell}}\bar{\bar{\mathbf{G}}}(\mathbf{k}_n) \cdot \left(e^{j\frac{2\pi}{a}ny_x}\hat{\mathbf{u}}_x\hat{\mathbf{u}}_x + e^{j\frac{2\pi}{a}ny_z}\hat{\mathbf{u}}_z\hat{\mathbf{u}}_z\right) \cdot (\overline{\overline{\varepsilon_r}} - \bar{\bar{\mathbf{I}}}) \cdot \mathbf{E}_{\mathrm{av}}. \tag{32}$$

The above formula establishes that $\mathbf{E}_{\mathrm{av},n}$ depends uniquely on $\mathbf{E}_{\mathrm{av}}$. By inserting (32) into (28a), we finally obtain the desired relation between the average fields

$$\mathbf{E}_{\mathrm{av,T}}(y;\mathbf{k}) = \bar{\bar{\mathbf{C}}}(y;\mathbf{k}) \cdot (\overline{\overline{\varepsilon_r}} - \bar{\bar{\mathbf{I}}}) \cdot \mathbf{E}_{\mathrm{av}} \tag{33}$$

$$\bar{\bar{\mathbf{C}}}(y;\mathbf{k}) = \sum_n e^{-j(k_y + \frac{2\pi}{a}n)y}\beta^2 \mathrm{V}_{\mathrm{cell}}\bar{\bar{\mathbf{G}}}(\mathbf{k}_n) \cdot \left(e^{j\frac{2\pi}{a}ny_x}\hat{\mathbf{u}}_x\hat{\mathbf{u}}_x + e^{j\frac{2\pi}{a}ny_z}\hat{\mathbf{u}}_z\hat{\mathbf{u}}_z\right). \tag{34}$$

The dyadic $\bar{\bar{\mathbf{C}}}(y;\mathbf{k})$ is calculated in closed analytical form in the Appendix.

In the remainder of this section, we calculate the average magnetic field $\mathbf{H}_{\mathrm{av,T}}(y;\mathbf{k})$. In analogy with (28a) we have

$$\mathbf{H}_{\mathrm{av,T}}(y;\mathbf{k}) = \sum_n \mathbf{H}_{\mathrm{av},n}e^{-j(k_y + \frac{2\pi}{a}n)y}. \tag{35}$$

From (3a) it is clear that $\eta\beta\mathbf{H}_{\mathrm{av},n} = \mathbf{k}_n \times \mathbf{E}_{\mathrm{av},n}$, and, therefore, we have

$$\eta\mathbf{H}_{\mathrm{av,T}}(y;\mathbf{k}) = \frac{1}{\beta}\left(\mathbf{k}_{//} + j\frac{d}{dy}\hat{\mathbf{u}}_y\right) \times \mathbf{E}_{\mathrm{av,T}}(y;\mathbf{k}) \tag{36}$$

where $\mathbf{k}_{//} = (k_x, 0, k_z)$.

IV. Numerical Results

In this section, we compare the results obtained with full wave numerical simulations with results from the theoretical analytical model developed before. The numerical results were obtained using the periodic moment method [1]. In the simulations it is assumed that the wire radius is $r_w = 0.01a$ and that $y'_L = y_z - 0.25a$ (see Fig. 5). For other values of y'_L the agreement between the numerical simulations and the analytical model is similar.

The normalized plasma wave number for $r_w = 0.01a$ is $\beta_0 a = 1.37$. The plasma frequency is given by $\omega_0 = \beta_0 c$, where c is velocity of light in vacuum. The physical meaning of the plasma frequency is that for $\omega < \omega_0$ the TM-z polarized waves in the associated 1-D-wire medium are cutoff (when the wires stand in air).

In Figs. 6 and 7, we plot the reflection coefficients of the co- and cross-polarized waves, respectively, versus normalized frequency, assuming TE-plane wave incidence. The direction of incidence is given by $(\cos\varphi\sin\theta, \cos\theta, \sin\varphi\sin\theta)$, i.e., θ is measured relatively to the y axis (see Fig. 5), and φ is the angle that the projection of the incident direction onto the xoz-plane makes with the x axis. We consider that $\varphi = 45°$, and that $\theta = 15°$ or $80°$. We admit that the wire slab is 1-cell thick (i.e., it consists of a set of vertical wires and a set of horizontal wires) and that the wires stand in free space: $\varepsilon_h = \varepsilon_0$. We plot the numerical results with full lines, and the results obtained with the analytical model with dashed lines.

As seen in Figs. 6 and 7, the agreement between the analytical and numerical results is very good, especially for $\omega/\omega_0 < 2.0$, which corresponds to $\lambda > 2.3a$, where λ is the wavelength of radiation in the host medium (air in this example). For $\lambda < 2.3a$, the agreement deteriorates relatively fast, especially for normal incidence and for the cross-polarization level. For $\lambda \approx 2.0a(\omega/\omega_0 \approx 2.3)$ the agreement is very bad for the cross-polarization. Thus, the range of the validity of the analytical

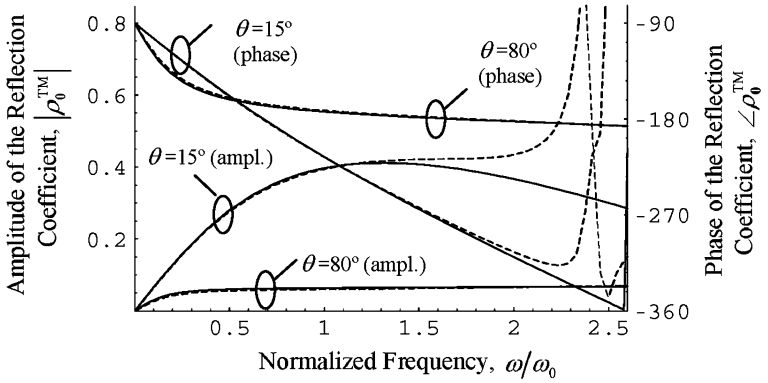

Fig. 7. Reflection coefficient (cross-polarized wave) versus normalized frequency: TE-incidence and $\varphi = 45°, \theta = 15°, 80°; \varepsilon_h = \varepsilon_0$. Full line: numerical results. Dashed line: analytical model.

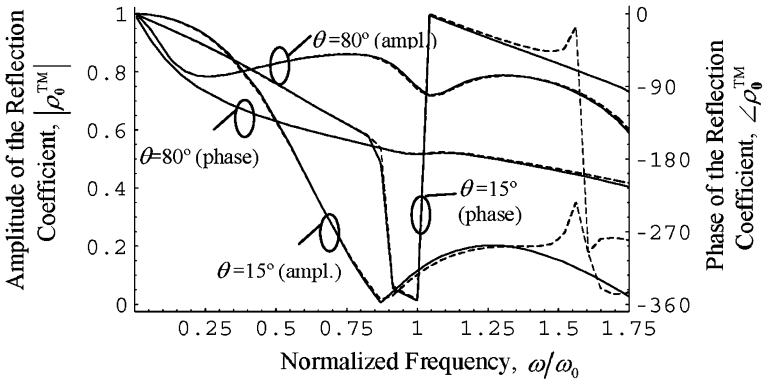

Fig. 8. Reflection coefficient (co-polarized wave) versus normalized frequency: TM-incidence and $\varphi = 45°, \theta = 15°, 80°; \varepsilon_h = 2.2\varepsilon_0$. Full line: numerical results. Dashed line: analytical model.

approach seems to be $\lambda > 2.0a$. This result is intuitively logical because the range of validity of the effective permittivity dyadic (9) is also expected to be approximately $\lambda > 2.0a$.

As shown in Fig. 7, the cross-polarization level increases with frequency. It is interesting to note that if we had identified the homogenized fields in the wire medium slab with those of the periodic unbounded structure, the analytical model would incorrectly predict that the cross-polarization level was exactly zero for $\varphi = 45°$ (note that when $\varphi = 45°, k_x = k_z$ and it can be shown that one of the modes given by (12) is such that $\mathbf{E}_{\mathrm{av},x} = \mathbf{E}_{\mathrm{av},z}$ and $\mathbf{H}_{\mathrm{av},x} = -\mathbf{H}_{\mathrm{av},z}$ and the other one is such that $\mathbf{E}_{\mathrm{av},x} = -\mathbf{E}_{\mathrm{av},z}$ and $\mathbf{H}_{\mathrm{av},x} = \mathbf{H}_{\mathrm{av},z}$). This clearly shows that the field $\mathbf{E}_{\mathrm{av,T}}$ cannot be identified with $\mathbf{E}_{\mathrm{av}}$, and that the correct homogenization of the problem involves averaging only the transversal coordinates, as described in the previous section. This proves that in general the homogenized thin screen cannot be identified with a slab of the homogenized bulk artificial material.

In Figs. 8 and 9, we plot the reflection coefficients of the co- and cross-polarized waves, respectively, versus normalized frequency, assuming TM-plane wave incidence, and that the wires are embedded in a dielectric slab with permittivity $\varepsilon_h = 2.2\varepsilon_0$. For small frequencies the wire mesh blocks the propagation of electromagnetic waves. Unlike in the TE- case, near the static limit the amplitude of the reflection coefficient decreases with the θ-angle. This property can be easily understood noting that for normal incidence and TM-polarization the incident electric field is parallel to the plane of the wires, whereas for wide angles it becomes progressively oriented along the y axis and thus the interaction with the wires is smaller.

As before, we obtain an excellent agreement between numerical simulations and the analytical model, especially for $\omega/\omega_0 < 1.25$, which corresponds to $\lambda > 2.5a$. For $\lambda \approx 2.0a (\omega/\omega_0 \approx 1.5)$ the agreement is very bad for the cross-polarization. Therefore, the range of validity also seems to be $\lambda > 2.0a$ in the dielectric case. Note that since λ is the wavelength in the host material the absolute range of validity of the model is worse in the dielectric case than in the case in which the wires stand in free-space.

A similarly good agreement between the numerical simulations and the analytical model is obtained for the transmission coefficients (both amplitude and phase), and for other incident directions.

The previous results prove that despite the wire structure being only one cell thick, it is possible to homogenize it with excellent results using the bulk material effective parameters and the homogenization procedure proposed in this paper.

Finally, in Fig. 10 we plot the reflected power versus the normalized frequency for TM- incidence, $\varphi = 45°$ and $\theta = 15°$, and structures with different thickness. We numerically simulated the cases in which the thickness of the wire slab is 1, 2, or 3 cells. The wires stand in free-space. As in the previous cases, we obtained a very good agreement between the numerical data and the analytical model. As the number of layers increases the response of the wire structure becomes increasingly

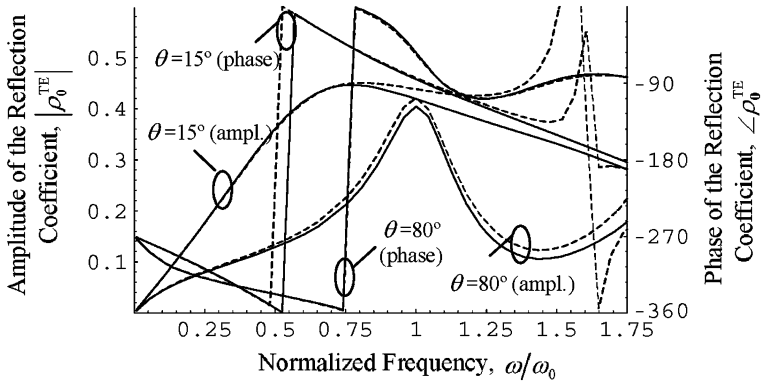

Fig. 9. Reflection coefficient (cross-polarized wave) versus normalized frequency: TM-incidence and $\varphi = 45°, \theta = 15°, 80°; \varepsilon_h = 2.2\varepsilon_0$. Full line: numerical results. Dashed line: analytical model.

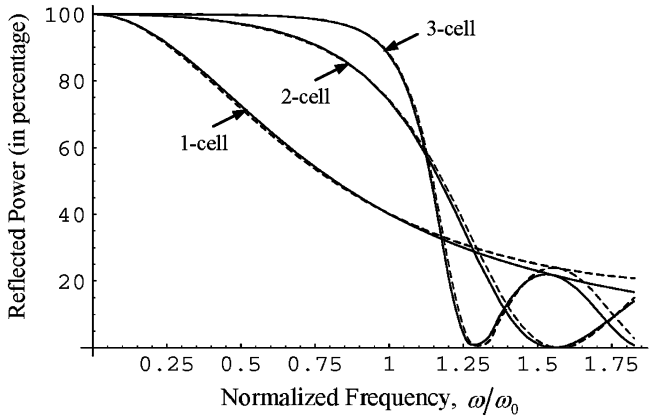

Fig. 10. Reflected power (in percentage) versus normalized frequency: TM-incidence and $\varphi = 45°, \theta = 15°; \varepsilon_h = \varepsilon_0$. The thickness is 1, 2, or 3 cells. Full line: numerical results. Dashed line: analytical model.

flat for $\omega/\omega_0 < 1$, i.e., below the cutoff frequency of the unbounded structure for normal incidence. Near the plasma frequency, $\omega/\omega_0 = 1$, the reflected power decreases steeply as the number of layers increase, and the band gap properties become increasing evident.

V. Conclusion

In this paper, we studied the canonical problem of scattering by a mesh of crossed wires. We proved that the bulk artificial material can be described (for long wavelengths) by a spatially dispersive permittivity dyadic. We proved that near the plasma frequency there exist two wave normal surfaces. We characterized the polarization of the homogenized electric fields, and compared the results with full wave numerical simulations. We discussed how the problem of scattering of plane waves by a "slab" of crossed wires must be homogenized. We proved that when the air-metamaterial interfaces are homogenized, the average fields in the artificial structure cannot be identified with those of the unbounded crystal. We derived the correct expression for the homogenized fields. We compared the results obtained with the proposed analytical model and full wave numerical results, with excellent agreement. We proved that our model is accurate for both polarizations, for normal incidence and wide incident angles, for different host materials, and also for both thin and thick structures. It is remarkable that even for 1-cell thick structures, the analytical model accurately predicts the amplitude and phase of the reflection and transmission coefficients (including the cross-polarization). We have shown that at least for this particular structure it is possible to characterize the scattering by thin screens directly from the effective parameters of the bulk artificial material.

We hope that the presented theory may contribute to a more profound understanding of the fundamentals of the homogenization theory of surfaces, which will certainly be an important tool for characterizing and designing emerging metamaterials and complex surfaces. The generalization of the proposed formalism to other planar structures with a single inclusion in the unit cell seems to be relatively straightforward, provided the effective parameters of the associated bulk material are known or can be computed.

Appendix

In this Appendix, we calculate the dyadic $\bar{\bar{\mathbf{C}}}$, defined by (34), in closed analytical form. To begin with, we note that from (29b) we can write

$$\bar{\bar{\mathbf{C}}}(y;\mathbf{k}) = \sum_n e^{-j(k_y+\frac{2\pi}{a}n)y} \frac{\beta^2\bar{\bar{\mathbf{I}}} - \mathbf{k}_n\mathbf{k}_{//}}{\mathbf{k}_n\cdot\mathbf{k}_n - \beta^2} \cdot \left(e^{j\frac{2\pi}{a}ny_x}\hat{\mathbf{u}}_x\hat{\mathbf{u}}_x + e^{j\frac{2\pi}{a}ny_z}\hat{\mathbf{u}}_z\hat{\mathbf{u}}_z\right) \quad \text{(A1)}$$

where $\mathbf{k}_n = \mathbf{k} + (0, n2\pi/a, 0)$ and $\mathbf{k}_{//} = (k_x, 0, k_z)$. We introduce the auxiliary scalar function

$$A(y;\mathbf{k}) = \sum_n \frac{e^{-j(k_y+\frac{2\pi}{a}n)y}}{|\mathbf{k}_{//}|^2 + \left(k_y + \frac{2\pi}{a}n\right)^2 - \beta^2}. \quad \text{(A2)}$$

It can be easily verified from the previous formulas that the dyadic $\bar{\bar{\mathbf{C}}}$ can be written as

$$\bar{\bar{\mathbf{C}}}(y;\mathbf{k}) = \left[(\beta^2\bar{\bar{\mathbf{I}}} - \mathbf{k}_{//}\mathbf{k}_{//}) - j\frac{d}{dy}\hat{\mathbf{u}}_y\mathbf{k}\right] \cdot \left(A(y-y_x;\mathbf{k})e^{-jk_yy_x}\hat{\mathbf{u}}_x\hat{\mathbf{u}}_x + A(y-y_z;\mathbf{k})e^{-jk_yy_z}\hat{\mathbf{u}}_z\hat{\mathbf{u}}_z\right). \quad \text{(A3)}$$

So, all we have to do is to evaluate (A2). To this end, we use the Poisson summation formula [18] to transform (A2) into a sum in the spectral domain. In this way, we obtain

$$A(y;\mathbf{k}) = \frac{a}{2\gamma}\sum_n e^{-\gamma|y-na|}e^{-jk_y na}, \quad \gamma = \sqrt{|\mathbf{k}_{//}|^2 - \beta^2} \tag{A4}$$

The above series can be summed in closed analytical form. Indeed, assuming that $|y| < a$, it can be rewritten as a sum of two geometrical series. We obtain

$$A(y;\mathbf{k}) = \frac{a}{2\gamma}\left(e^{-\gamma|y|} + \sum_{\pm}\frac{e^{\pm\gamma y}}{e^{(\gamma\pm jk_y)a}-1}\right), \quad |y| < a. \tag{A5}$$

In the previous formula, the sum with index "$\pm$" stands for the sum of two terms, one with "$+$" sign and other with the "$-$" sign. We stress that (A5) is valid only for $|y| < a$. However, from the definition (A2), $A(y;\mathbf{k})$ is a pseudo-periodic function with wave number k_y. More specifically, $A(y;\mathbf{k})\exp(jk_y a)$ is a periodic function of y. Thus, it is clear that (A5) can be used to evaluate $A(y;\mathbf{k})$ in an arbitrary point of space, making use first of the pseudo-periodicity to reduce the point to the unit cell $|y| < a/2$.

REFERENCES

[1] T. K. Wu, Ed., *Frequency Selective Surface and Grid Array*. New York: Wiley, 1995, ch. 1.

[2] R. F. J. Broas, D. F. Sievenpiper, and E. Yablonovitch, "A high-impedance ground plane applied to a cellphone handset geometry," *IEEE Trans. Microw. Theory Tech.*, vol. 49, no. 7, pp. 1262–1265, Jul. 2001.

[3] S. Clavijo, R. E. Díaz, and W. E. McKinzie III, "Design methodology for sievenpiper high-impedance surfaces: An artificial magnetic conductor for positive gain electrically small antennas," *IEEE Trans. Antennas Propag.*, vol. 51, no. 10, pp. 2678–2690, Oct. 2003.

[4] M. I. Kontorovich, V. I. Petrunkin, N. A. Esepkina, and M. I. Astrakhan, "Reflection factor of a plane electromagnetic wave reflecting from a plane wire grid," *Radio Eng. Electron Phys.*, no. 2, pp. 222–231, 1962.

[5] V. V. Yatsenko, S. A. Tretyakov, S. I. Maslovski, and A. A. Sochava, "Higher order impedance boundary conditions for sparse wire grids," *IEEE Trans. Antennas Propag.*, vol. 48, no. 5, pp. 720–727, May 2000.

[6] J. R. Wait, "Impedance of a wire grid parallel to a homogeneous interface," *IRE Trans. Microw. Theory Tech.*, pp. 99–102, Apr. 1957.

[7] J. L. Young and J. R. Wait, "Note on the impedance of a wire grid parallel to a homogeneous interface," *IEEE Trans. Microw. Theory Tech.*, vol. 37, no. 7, pp. 1136–1138, Jul. 1989.

[8] R. R. DeLyser, "Use of equivalent boundary conditions for the solution of a class of strip grating structures," *IEEE Trans. Antennas Propag.*, vol. 41, no. 1, pp. 103–105, Jan. 1993.

[9] K. W. Whites and R. Mittra, "An equivalent boundary-condition model for lossy planar periodic structures at low frequencies," *IEEE Trans. Antennas Propag.*, vol. 44, no. 12, pp. 1617–1629, Dec. 1996.

[10] A. A. Kishk and P.-S. Kildal, "Asymptotic boundary conditions for strip-loaded scatterers applied to circular dielectric cylinders under oblique incidence," *IEEE Trans. Antennas Propag.*, vol. 45, no. 1, pp. 51–56, Jan. 1997.

[11] A. A. Kishk, P.-S. Kildal, A. Monorchio, and G. Manara, "Asymptotic boundary condition for corrugated surfaces, and its application to scattering from circular cylinders with dielectric filled corrugations," *Proc. Inst. Elect. Eng. Microwave Antennas Propag.*, vol. 145, no. 1, pp. 116–122, Feb. 1998.

[12] J. L. Blanchard, E. H. Newman, and M. Peters, "Integral equation analysis of artificial media," *IEEE Trans. Antennas Propag.*, vol. 42, pp. 727–731, May 1994.

[13] S. Datta, C. T. Chan, K. M. Ho, and C. M. Soukoulis, "Effective dielectric constant of periodic composite structures," *Phys. Rev. B*, vol. 48, pp. 14 936–14 943, 1993.

[14] F. Wu and K. Whites, "Quasistatic effective permittivity of periodic composites containing complex shaped dielectric particles," *IEEE Trans. Antennas Propag.*, vol. 49, no. 8, pp. 1174–1182, Aug. 2001.

[15] P. A. Belov, S. A. Tretyakov, and A. J. Viitanen, "Dispersion and reflection properties of artificial media formed by regular lattices of ideally conducting wires," *J. Electromagn. Waves Applicat.*, vol. 16, no. 8, pp. 1153–1170, 2002.

[16] M. Silveirinha and C. A. Fernandes, "Effective permittivity of metallic crystals: A periodic Green's function formulation," *Electromagn.*, vol. 23, no. 8, pp. 647–664, 2003.

[17] P. A. Belov, R. Marqués, S. I. Maslovsky, I. S. Nefedov, M. Silveirinha, C. R. Simovsky, and S. A. Tretyakov, "Strong spatial dispersion in wire media in the very large wavelength limit," *Phys. Rev.*, vol. B 67 113 103, no. 1–4, 2003.

[18] R. E. Collin, *Field Theory of Guided Waves*, 2nd ed. New York: IEEE Press, 1991.

[19] M. Silveirinha and C. A. Fernandes, "A hybrid method for the efficient calculation of the band structure of 3D metallic crystals," *IEEE Trans. Microwave Theory Tech.*, no. 3, pp. 889–902, Mar. 2004.

[20] K. Sakoda, *Optical Properties of Photonic Crystals*. New York: Springer Series in Optical Sciences, 2001, vol. 80.

Mário G. Silveirinha (S'99–M'03) received the "Licenciado" degree in electrical engineering from the University of Coimbra, Coimbra, Portugal, in 1998, and the Ph.D. degree in electrical and computer engineering from the Instituto Superior Técnico (IST), Technical University of Lisbon, Lisbon, Portugal, in 2003.

His research interests include propagation in photonic crystals and homogenization and modeling of metamaterials.

Carlos A. Fernandes (S'86–M'89) received the "Licenciado," M.Sc., and Ph.D. degrees in electrical and computer engineering from the Instituto Superior Técnico (IST), Technical University of Lisbon, Lisbon, Portugal, in 1980, 1985, and 1990, respectively.

He joined the IST in 1980, and since 1993 has been an Associate Professor at the Department of Electrical and Computer Engineering in the areas of microwaves, radiowave propagation, and antennas. Since 1993, he also been a Senior Researcher at the Instituto de Telecomunicações, where he is the Coordinator of the Wireless Communications scientific area. He has been the Leader of the antenna activity in National and European Projects as RACE 2067-MBS (Mobile Broadband System), and ACTS AC230-SAMBA (System for Advanced Mobile Broadband Applications). He has co-authored a book, a book chapter, and several technical papers in international journals and conference proceedings, in the areas of antennas and radiowave propagation modeling. His current research interests include artificial dielectrics, dielectric antennas for millimeterwave applications, and propagation modeling for mobile communication systems.